Chapter 2: Review of Microbolometer

In this chapter, the basics of microbolometer theory and micromachining are covered. The theory of microbolometer detectors is discussed in detail, as well as their performance limitation. Techniques to realize better performance of micromachined microbolometers are explained.

2.1 Microbolometer Operation

A simple model of the heat equation for a temperature rise due to a time varying radiation source is [1]

$$C\frac{d(\Delta T)}{dt} + G(\Delta T) = P_{absorbed}e^{jwt}\ , \tag{2.1}$$

where C is the heat capacity, G is the thermal conductance ($1/Z_{thermal}$), $P_{absorbed}$ is the absorbed peak radiation power, and $\boldsymbol{w}$ is modulation frequency which can be set by a mechanical chopper.

A steady state solution to Eqn.2.2 is

$$\Delta T = Z_{thermal} \cdot \frac{1}{\sqrt{1+\boldsymbol{w}^2\boldsymbol{t}^2}} \cdot P_{absorbed}\ , \tag{2.2}$$

where τ is the thermal time constant equal to C/G $(CZ_{thermal})$, and $P_{absorbed}$ is the absorbed power.

If the frequency of incoming radiation is small ($\omega\tau < 1$), the temperature rise ΔT will be independent of heat capacity C. For a fast response, the heat capacity must be minimized by reducing the volume of bolometer. With no radiation applied, the temperature of the bolometer is affected only by Joule heating from the bias current and the transfer of heat out of the bolometer.

As the temperature of a microbolometer is changed, for example from exposure to infrared radiation, there is a proportional change in electrical resistance. By application of a known bias current, the change in microbolometer resistance can be converted to an easily measured potential difference.

Thermal radiation detectors include an absorbing element and a heat sink (Fig.2.1 (a)). The heat capacity C of the absorbed element describes the amount of electromagnetic radiation converted to heat whereas the thermal conductance G models the transfer of energy from the element to the sink. Upon exposure to incident power $P_{incident}$, temperature T_B of this absorbing element initially increases with time at rate $dT_B/dt = P_{incident}/C$ and approaches the limiting value $T_B = T_S + P_{incident}/G$ with the thermal time constant $\tau = C/G$ for simple, single time constant systems. When the source of the radiation is removed, the microbolometer returns to T_s with the same time constant τ.

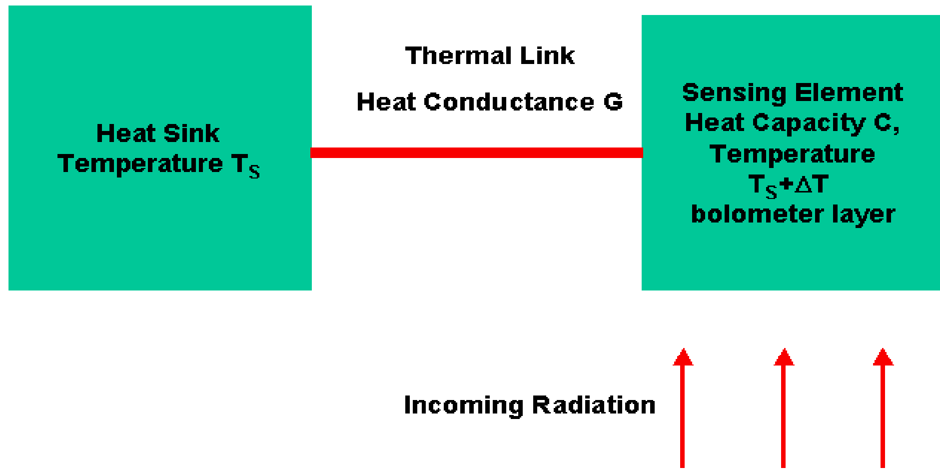

(a)

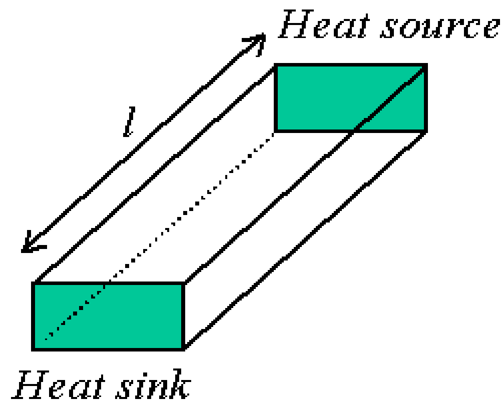

(b)

Figure 2.1 (a) Incoming radiation causes the instantaneous temperature of the sensing element to be T_s + ?T. The element is connected via a conducting link through conductance G to the heat sink, which remains at temperature T_s. (b) bolometer geometry for a "long" rectangular device.

Since thermal capacitance is approximately proportional to bolometer volume, reduction of bolometer size leads to an increase in the speed of the devices. Thermal conductance is related to bolometer geometry for a “long” rectangular device by

$$G_{dc} \propto k \frac{A_{bolo}}{l} \quad \text{and} \quad C \propto M\rho c \,, \tag{2.3}$$

where k is the thermal conductivity of material, A_{bolo} is the cross sectional area of thermal link of bolometer, l is the length of bolometer, M is the volume of the bolometer, ρ is the density and c is the specific heat.

Using Eqn. 2.2, the signal voltage V generated by a change in temperature $(T_B - T_S)$ for microbolometer detector is

$$V = I_b \cdot \frac{dR}{dT} \cdot \Delta T = I_b \cdot \frac{dR}{dT} \cdot P_{absorbed} \cdot Z_{thermal} \cdot \frac{1}{\sqrt{1+\omega^2\tau^2}} \,, \tag{2.4}$$

where I_b is the bias current, and ${}^{dR}\!/_{dT}$ is the change in resistance of the bolometer for given change in T.

2.2 Detector Performance Characterization

2.2.1 Responsivity

The performance of bolometric detectors is characterized by certain figures of merit which include responsivity, noise equivalent power (NEP), and

detectivity. The fundamental purpose of a microbolometer detector is to convert an incoming optical signal into an electrical signal. The term *responsivity* is used to describe the amplitude of the electrical signal with respect to the incident flux [1].

$$\Re(\boldsymbol{l}) = \frac{V_{out}}{\boldsymbol{f}_{incident}} = \frac{V_{out}}{E \cdot A_d} \quad \text{[V/W]}, \tag{2.5}$$

where V_{out} is the detector output voltage, $\boldsymbol{F}_{incident}$ is the incident power in Watts, E is the incident irradiance in Watt per square centimeter, and A_d is the detector active area in square centimeters.

For the purpose of analysis, the voltage responsivity can be rewritten as the root-mean-square (rms) signal voltage output per unit radiant power incident upon the detector. The responsivity, $\Re$, is thus given by [2]

$$\Re = \frac{V}{P_{incident}} = I_b \cdot \frac{dR}{dT}\frac{dT}{dP} \cdot \frac{P_{absorbed}}{P_{incident}} = I_b \cdot Z_{thermal} \cdot \frac{dR}{dT}\frac{1}{\sqrt{1+\boldsymbol{w}^2\boldsymbol{t}^2}} \cdot \boldsymbol{h}, \tag{2.6}$$

where $\boldsymbol{h}$ is the coupling efficiency of incident wave.

If dR/dT *[V/W]* is constant over the temperature range considered, the temperature change in the device is proportional to change in dissipated power. One characteristic of a microbolometer is the linear relationship between resistance and dissipated power over the operating temperature range.

If responsivity is characterized in the DC, the responsivity is

$$\Re_{dc} = I_b \frac{dR}{dP} = I_b \frac{dR}{dT} \frac{dT}{dP_{absorbed}} . \tag{2.7}$$

The DC Resistance measured as a function of power therefore provides enough information to determine $\hat{\boldsymbol{A}}$ and thermal conductance G for the device. In DC characterization, the source of absorbed power could be just the joule heating from bias current. This method of characterization can be helpful to estimate the performance of bolometer for a time varying source of radiation.

To increase the responsivity, bias current cannot be increased infinitely. It is limited mainly by Joule heating and detector instability, which will be explained later [3].

2.2.2 Noise Equivalent Power (NEP) and Detectivity (D*)

The responsivity of a microbolometer is related to the voltage signal level and the incident flux measured on the detector. However, large responsivity does not necessarily mean that the microbolometer can easily discern small optical signal changes. Hence, a more appropriate measure of a detector's performance is how well it extracts a signal from the surrounding noise. That characteristic is referred as noise equivalent power (NEP).

Noise equivalent power is defined as the rms value of sinusoidally modulated radiant power falling on the detector required to produce signal to noise ratio of one ($S/N = 1$). NEP is most frequently specified at bandwidth of 1

Hz, and expressed in units of watts/$Hz^{1/2}$ [2]. NEP is related to the noise voltage (V_n) and responsivity ($\hat{\boldsymbol{A}}$) by

$$NEP = \frac{V_n}{\Re}. \tag{2.8}$$

The detectivity, or D^*, is the reciprocal of the NEP, normalized to detector area 1 cm^2, and 1 Hz electrical bandwidth.

$$D^* = \frac{{A_{bolo}}^{1/2} b^{1/2}}{NEP} \tag{2.9}$$

where: D* = detectivity in cm-$Hz^{1/2}$/watt, A = detector area in cm^2, and b = post-detection electrical bandwidth.

2.3 Performance Limitations

Due to the low signal voltage from microbolometer devices, the most important figure of merit to consider during design and optimization is responsivity. According to the responsivity equation derived above (Eqn.2.6), responsivity can be optimized by maximization of the bias current and detector coupling efficiency. By breaking these terms into physical constants, the role of the microbolometer's material properties and structures becomes much clearer.

$$\Re = I_b \cdot Z_{thermal} \cdot \boldsymbol{a} \cdot R_{bolo} \cdot \frac{1}{\sqrt{1 + \boldsymbol{v}^2 \boldsymbol{t}^2}} \cdot \boldsymbol{h} \tag{2.10}$$

where α is the temperature coefficient of resistance (TCR).

Equation (2.10) indicates that responsivity depends on bias current, thermal conductance, the temperature coefficient of resistance (TCR), and coupling efficiency.

2.3.1 Thermal impedance

Heat transfer takes place in three forms: radiation, convection, and conduction. Radiant heat transfer is usually small due to small size of devices. Since radiated power (W) depends upon the temperature according to Stefan-Boltzmann's law,

$$W = \sigma T^4, \quad (2.11)$$

and the temperature of a microbolometer from room temperature radiant transfer is usually fairly low.

Convection can be significant for devices larger than tens of microns, but is negligible at low pressure. Wood and Eriksson reported a 2 - 3 order difference between the thermal impedance measured in a vacuum (75 mTorr) measured at ambient pressure [4] [5]. Thermal conductance, the reciprocal of thermal impedance, can be the limiting mechanism of heat flow from small body of detector.

With the use of the Wiedemman-Franz Law, which explains the relationship between thermal and electrical conductivity, the thermal conductance can be thought of in terms analogous to the electrical conductance [6]. The thermal conductivity for various metals is listed in table 2.1.

To maximize the responsivity, the thermal conductance of the bolometer must be minimized (thermal impedance maximized) as shown Eqn. 2.9. Therefore, cross sectional area must be decreased and the length of the thermal link must be increased.

	Thermal conductivity
Silicon (Bulk)[1]	~ 1.3 W/cm-K
Silicon Oxide (SiO_2)[1]	~ 0.014 W/cm-K
Silicon Nitride (Si_3N_4)[1]	~ 0.032 - 0.0385 W/cm-K
Bismuth (Thin film)[2]	~0.015 – 0.018 W/cm-K
Bismuth (Bulk film)[3]	~ 0.0792 W/cm-K
Gold (Au)[4]	~ 3.15 W/cm-K
Chromium (Cr)[5]	~ 0.019 W/cm-K

Table 2.1 Bulk thermal conductivity of various materials used in microbolometers at 300K. These values are for bulk material; thin films may have different characteristics.

---

[1] As reported by Y.S. Touloukian [7]
[2] As reported by Abrosimov et al. [8]
[3] CRC Handbook of Chemistry and Physics, 64th edition, CRC Press, 1984
[4] Material Handbook for Hydrid Microelectronics, Artech House, 1988
[5] The program of material properties data base (MPDB), 2000

In addition, for larger thermal impedance, freestanding films can be formed using specific micromachining techniques such as bulk and sacrificial processes. It has been found that the responsivity of a microbolometer can be increased by the use of suspended bridges that prevent contact between the detector and substrate. With micromachined freestanding microbridge structure, it is possible to achieve a thermal impedance as high as 1 M K/W in a vacuum [5][9].

2.3.2 Temperature coefficient of resistance

The temperature coefficient of resistance (TCR) is critical in bolometer material selection. There has been a large amount of research to find a material with a large and stable TCR. The TCR can be written as

$$TCR = \alpha = \frac{1}{R_{bolo}} \cdot \frac{dR_{bolo}}{dT}. \qquad (2.12)$$

Vanadium oxide is currently the most popular and promising material for room temperature bolometer applications. For low temperature applications, the superconducting bolometer exploits the resistive transition at the superconducting threshold where the TCR is maximum. Table 2.2 shows TCR of several materials.

Depending on material characteristics, some materials (usually metal) show a positive TCR, while others have a negative TCR. In terms of detector stability issue which is explained in section 2.3.3, a negative TCR is favored due to current bias comparing to those materials with a positive TCR. In general, the

negative TCR of materials is a consequence of two competing mechanisms [6]. First, the carrier concentration increases with increasing T. Second, the carrier mobility decreases with increasing temperature. Therefore, the resulting sign of differential conductivity over temperature is proportional to the product of carrier concentration and carrier mobility at a given temperature range. A desirable microbolometer material has large TCR values with negative TCR at operating temperature.

	TCR
Y-Ba-Cu-O (YBCO)	~ + 0.5 - 1 K^{-1} (Transition at ~88K)
Vanadium Oxide (V_{ox})	~ - 0.015 - 0.028 K^{-1} (Room temp.)
Silver (Ag)	~ + 0.0037 K^{-1} (Room temp.)
Nickel (Ni)	~ + 0.005 K^{-1} (Room temp.)
Gold (Au)	~ + 0.0036 K^{-1} (Room temp.)
Bismuth (Bi)	~ - 0.003 K^{-1} (Room temp.)
Chrome (Cr)[6]	~ - 0.000522 K^{-1} (Room temp.)

Table 2.2 Comparison of TCR of various materials [3].

[6] TCR of Chrome is measured by Yoo

2.3.3 Bias current

From the derived responsivity relationship (Eqn.2.6), by increasing the bias current, a higher responsivity can be achieved. The maximum bias current is likely to be limited by one of the following factors which lead to microbolometer failure: thermally induced current due to joule heating, high filament current density which leads to electromigration failure in the detector element, and detector instability. Lewis described these microbolometer bias current limitations in more detail [3]. In this chapter, the explanation and examination of these factors will be made with respect to the micromachinined microbolometer, in particular those fabricated with a free-standing support leg.

The power dissipated in the microbolometer detector consists of incoming radiation and joule heating from the bias current. However, the power dissipated in the detector is predominantly due to joule heating from the bias source. Therefore, the maximum allowable detector bias current can be restricted according to the maximum allowed temperature rise

$$\Delta T_{MAX} = T_{MAX} - T_{AMB} = P_{MAX} \cdot Z_{thermal} = I_{MAX}^{2} \cdot R_{bolo} \cdot Z_{thermal}, \qquad (2.13)$$

where T_{MAX} is the maximum allowable temperature, T_{AMB} is the ambient temperature, P_{MAX} is the maximum allowable DC bias power, and I_{MAX} is the maximum allowable bias current in terms of the maximum allowed temperature rise.

Hence, the maximum allowable detector bias current is

$$I_{MAX} = \sqrt{\frac{\Delta T_{MAX}}{R_{bolo} \cdot Z_{thermal}}} . \tag{2.14}$$

Using Eqn.2.14 and 2.10, the relationship between bias current and responsivity is found to be

$$\Re = \sqrt{\Delta T_{MAX}} \cdot \sqrt{R_{bolo}} \cdot \sqrt{Z_{thermal}} \frac{\boldsymbol{a}}{\sqrt{1 + \boldsymbol{w}^2 \boldsymbol{t}^2}} \cdot \boldsymbol{h} . \tag{2.15}$$

The above relations Eqn.2.12-2.15 can be useful in evaluating potential detector materials and configurations. For example, the responsivity may be improved by using detector materials that can withstand high temperature**.** Therefore, materials resistant to melting are good candidates to be used in detectors. The maximum temperature difference can also be increased by lowering ambient temperature. This is also likely to improve NEP by reducing the thermally induced component of noise. Responsivity may be increased easily by choosing a high resistance detector.

With the assumption that the maximum allowable current is determined by the maximum allowable bias current rather than a maximum allowable temperature, another mechanism for device failure is electromigration [10]. In the case of the free-standing microbridge structure, the maximum allowable current can be restricted to one of the supporting leg structures. Therefore, it can be related to the maximum current density according to

$$I_{\max} = J_{\max} \cdot t_{leg} \cdot w_{leg}, \tag{2.16}$$

where J_{max} is the maximum current density, t_{leg} is the thickness of supporting leg of the microbolometer, and w_{leg} is the width of bridge of the microbolometer. Therefore, if thermal impedance is

$$Z_{thermal} = \frac{l_{leg}}{t_{leg} \cdot w_{leg} \cdot \kappa_{leg}}, \tag{2.17}$$

where κ_{leg} is the thermal conductivity of legs.

Then, responsivity is

$$\Re = J_{\max} \cdot \frac{R_{bolo} \cdot l_{leg}}{\kappa_{leg}} \cdot \frac{\alpha}{\sqrt{1+\omega^2\tau^2}} \cdot \eta. \tag{2.18}$$

The thermal impedance will also be dependant on the length to width ratio of the supporting leg of the detector. For a given detector material, the length to width ratio of detector will determine the maximum responsivity of the device.

Another important issue that limits responsivity through bias current is stability under constant bias conditions. If the device is biased at constant current, positive or negative feedback results, depending on whether the detector has a positive or negative temperature coefficient of resistance. The feedback is due to the absorption of incident radiation affecting the bias power by changing detector

resistance. For example, with constant current bias and a positive coefficient of resistance, incident power will increase the resistance of the detector. Since the bias current is held constant, this will increase the bias power, thus further increasing the resistance and further increasing the bias power.

The relation for stable operation with positive TCR is [3]

$$\Re \cdot I_b < 1 . \tag{2.17}$$

This relation can be rewritten

$$I_{MAX} \leq \frac{1}{\sqrt{Z_{thermal} \cdot \boldsymbol{\alpha} \cdot R_{bolo}}} . \tag{2.18}$$

The criterion defined in Eqn.2.17 should be considered when modeling a detector that has a positive TCR material such as a superconductor microbolometer. However, if a bolometer material with negative TCR is chosen instead detector stability is not an issue.

2.3.4 Coupling efficiency ($P_{absorbed}/P_{incident}$)

The quantity $\boldsymbol{\eta}$ ($P_{absorbed}/P_{incident}$) introduced in section 2.2.1 is the absorption efficiency of the microbolometer detector. By maximizing the coupling efficiency an absorption enhanced device can be fabricated. By modulating absorption of the incoming optical signal, the amount of absorbed power by the device can be adjusted, and the construction of a wavelength

selective device is possible. There are two different approaches to control coupling efficiency. The first is to use a microbolometer material that responds to a specific wavelength [10]. The second is to alter the structure of the microbolometer to make the coupling efficiency a function of wavelength. For this structural approach, a device model and the method of its fabrication will be explained in chapters 3 and 4.

2.4 Overview of Silicon Micromachining Technique

Significant improvement in thermal performance is achieved by removing the substrate from the bolometer, supporting it with long and narrow suspension legs to increase the thermal impedance by use of micromachining technique. The common feature of micromachining can be explained in this section.

A micromachining technique refers to the technologies and method of fabricating three dimensional structures and devices with physical dimensions on the order of micrometers. Peterson summarized the excellent mechanical material characteristics of silicon for use in microstructures (Table 2.3) [11]. The yield strength of silicon is two times higher and young's modulus is very equivalent to that of steel. The density is very close to aluminum but only one third that of steel. Due to its entirely elastic characteristic, silicon does not have mechanical hysterisis. Mechanical stability of deposited or grown layers on silicon substrate can be optimized by several methods as well. The typical residual stress of silicon nitride and silicon oxide deposited by Low Pressure Chemical Vapor Deposition (LPCVD) has a high tensile stress, about 1×10^{10} dyne/cm^2 and low compressive

stress about 1 x 10^{10} dyne/cm^2, respectively [12]. By changing the deposition method to Plasma Enhanced Chemical Deposition (PECVD), the residual tensile stress of silicon nitride can be less than 2 x 10^{10} dyne/cm^2 [12]. In addition, by alternating layers of material with opposite residual stress polarity of silicon nitride and silicon oxide, the residual stress level can be reduced even further at the expense of increasing process complexity. For polysilicon, the residual stress can be reduced by high temperature annealing (usually 1000 – 1200 °C) for several hours [13][14].

Property	Measure
Crystal structure	Diamond, 8 atoms/unit cell
Melting Point	1415 °C
Thermal expansion	2.5 x 10^{-6}/°C
Density	2.3 g/cm^3
Young modulus	1.9 x 10^{12} dyne/cm^2
Yield strength	6.9 x 10^{10} dyne/cm^2
Knoop hardness	850 kg/m^2

Table 2.3 Important mechanical properties of silicon crystal [11].

Generally, there are two basic techniques associated with silicon micromachining: bulk micromachining and surface micromachining. Both of these techniques are compatible with well-established IC technology, which means low cost and high volume manufacturing processes are possible for microelecromechanical system (MEMS). Other than these techniques, there are several additional techniques can be exploited to build three-dimensional structure such as wafer bonding [14] and LIGA [14].

2.4.1 Bulk micromachining techniques

The most common process for removing silicon substrate in bulk micromachining is to use wet anisotropic (i.e. orientation-dependent) silicon etching. Many anisotropic etchants can be used for silicon, such as EthyleneDiamine Pyrocatechol (EDP), Potassium Hydroxide (KOH) and Cesium Hydroxide (CsOH) [14]. KOH is more frequently used for anisotropic etching because it exhibits a much higher anisotropic (100)-(111) etch ratio (400:1) [11]. Depending on the choice of etchants, silicon dioxide or silicon nitride can be used as an etch mask, since a photoresist is easily peeled off at on early stage of etching and also can not endure long wet etching at high temperature. If KOH is used, silicon dioxide is not suitable for etch masks because it etches too quickly. Silicon nitride made by Low Pressure Chemical Vapor Deposition (LPCVD) can endure for several hours in a KOH solution as a mask. However, silicon nitride made by Plasma Enhanced Chemical Vapor Deposition (PECVD) is less selective compared with silicon nitride made by LPCVD. The etching rate of silicon nitride

made by LPCVD is observed to be about 10 Å/hour at 110°C, while that of silicon nitride made by PECVD is approximately 400 Å/hour at 80°C by Yoo in the microelectronic research center. PECVD silicon nitride is unsuitable as a mask for removing the entire substrate (250µm -500µm) beneath the membrane.

Figure 2.2 shows a schematic drawing of the fabrication procedure of a planar membrane. Due to the orientation dependency of the etch rate, the etched surface is bounded by the (111) planes, which have the slowest etch rates. The final length of the square dielectric membrane is determined by the etch time and the thickness of the silicon wafer since the etching produces (111) planes as the side walls at an angle of 54.7°. Dielectric layers were used for the etch stop layer to control and determine the accurate dimensions in the etching process. Another etch stop mechanism involves the use of high boron concentration of approximately 2.5×10^{19} cm^{-3}. Above this critical concentration, the etch rate starts to drop and a final reduction of three orders of magnitude in the etch rate is achieved with a about the concentration of 10^{21} cm^{-3} [14].

2.4.2 Surface micromachining techniques

Surface micromachining techniques produce a three dimensional microstructure in layers of thin films on the surface of a substrate. The process would typically employ films of two different materials, which are deposited and etched in sequence. Finally the sacrificial material is wet etched away to release the structure. The structural complexity and fabricating difficulty increases with increasing numbers of material layers.

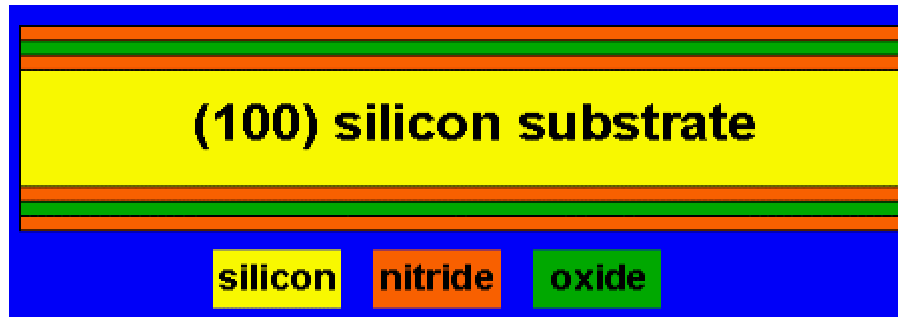

(a)

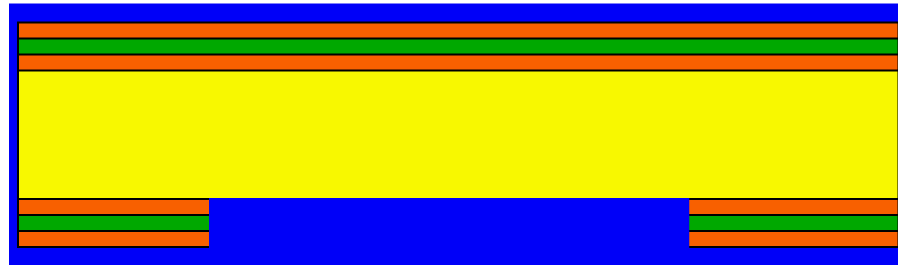

(b)

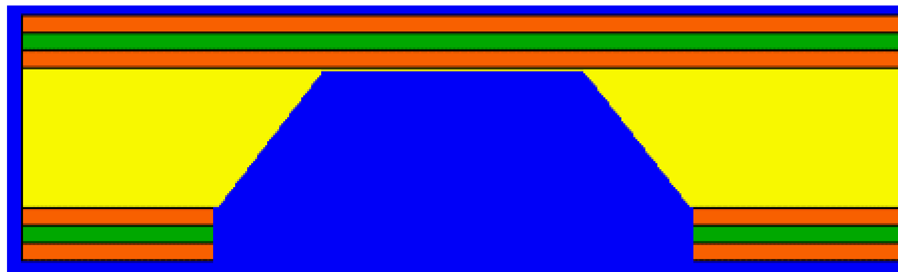

(c)

Figure 2.2 Schematic view of the fabrication procedure for a planar diaphragm using bulk micromachining. (a) Deposition of silicon nitride, silicon dioxide, and silicon nitride by LPCVD. (b) Patterning and plasma etching on the backside of wafer. (c) Anisotropic etching using KOH at 110 °C.

A variety of different cavities can be fabricated on the surface of silicon substrate using surface micromachining techniques. As shown in Fig. 2.4a, the size of the cavity is determined by the volume of the initially deposited dielectric film (the lost layer). A mold layer is then deposited over the surface of the silicon wafer (Figure 2.3b). A window is dry etched through the coating layer, and the wafer is then immersed in a wet etchant that removes the sacrificial layers selectively, leaving a windowed chamber as shown in figure 2.3c.

As the process becomes more complex, the release of freestanding structures becomes the most challenging issue for surface micromachining in the MEMS industry. During the rinse and dry cycle that follows the sacrificial etching process, the evaporating rinse solution creates a large capillary force that tends to draw the mold layer toward the underlying substrate [13][14]. As a result, the microstructure will adhere to the wafer surface after the rinse and dry cycle is completed. This layer separation failure mode is common, which make it difficult to achieve high yield necessary for mass manufacturing. This issue will be discussed in more detail in chapter 4.

Using micromachining techniques described above, examples of device are demonstrated in Fig.5.4 and Fig.5.5, which are done by author. Even though the characteristic of device different, the common features of technique are applicable for fabricating the microbolometer.

A micromachined inductor constructed to improve the inductor performance by removing the substrate conductivity as shown in Fig.2.5.

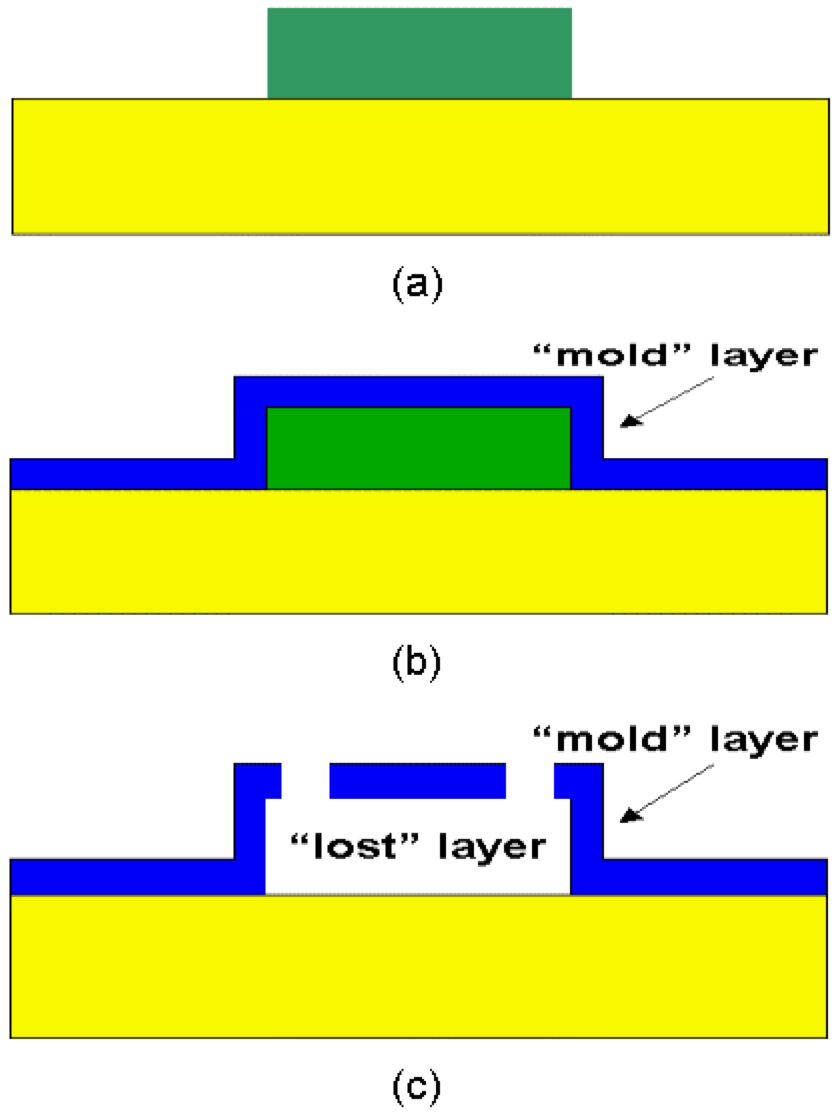

Figure 2.3 Schematic view of fabrication procedure for typical surface micromachining. (a) Deposit and pattern the sacrificial layer; (b) Overcoat to make mold. (c) Selectively remove sacrificial layer and release the structure (lost layer is usually either polysilicon or oxide).

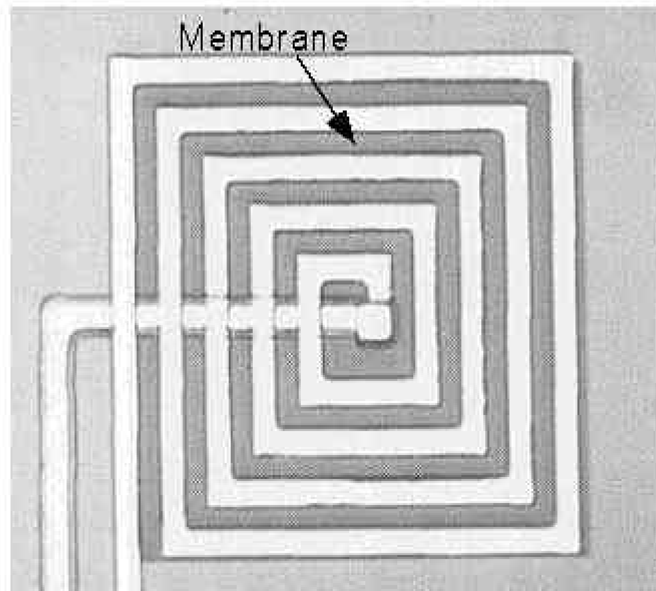

Figure 2.4 The micromachined inductor[7] on a membrane made by metal wet etching process. The dark square is the membrane with silicon substrate removed from underneath inductor. This improves the inductor performance by removing the substrate conductivity effect [15].

Due to the effect of substrate conductivity, the performance of inductor is degraded at the high frequency. The micromachined inductor is fabricated on a $Si_3N_4/SiO_2/Si_3N_4$ membrane with removal of the underlying substrate by KOH anisotropic etching.

The micromachined storage wells were constructed for use in an artificial tongue as shown in Fig.2.5. Electronic tongue is capable of discrimination of

[7] Seung-Jin Yoo, "Modeling and Fabrication of Micromachined Inductors," MS thesis, 1997.

different analytes, toxins, and bacteria have become increasingly important for real time diagnosis of pathogens. In particular, molecules that change their optical properties when exposed to the target material provide the potential for highly sensitive detection.

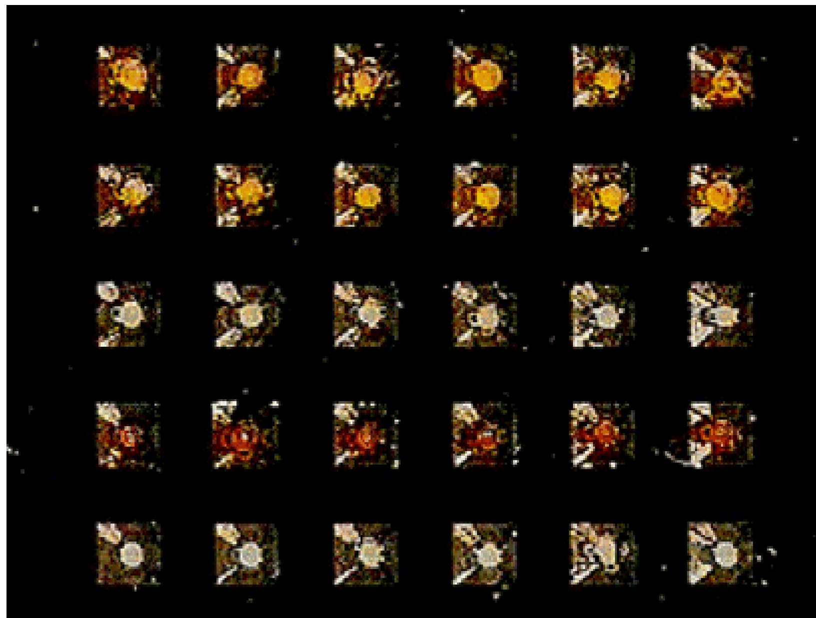

Figure 2.5 The micromachined storage wells[8] for chemical sensing beads in an artificial tongue using bulk micromachining [16].

[8] S. Savoy, J.J. Lavigne, S.-J. Yoo, and et al. "Solution based analysis of multiple analytes by a sensor array: toward the development of an electronic tongue," SPIE Conference on Chemical Microsensors and Applications, SPIE Vol.3539, Bonston, MA, Nov. 4, 1998.

2.5 Summary

This chapter reviews the practical aspect in the design, fabrication, and the characterization of microbolometer. Included are the operation of microbolometer, figures of merit, performance limitations, and silicon micromachining techniques. This information provides a background for the discussion of various issues encountered during fabrication and characterization of micromachined microbolometer with a power coupling enhanced structure.